Journal of Nuclear Materials 378 (2008) 70–78

Contents lists available at ScienceDirect

Journal of Nuclear Materials

journal homepage: www.elsevier.com/locate/jnucmat

Diffusion of radiogenic helium in natural uranium oxides

Danièle Roudil [a,*], Jessica Bonhoure [b], Raphaël Pik [c], Michel Cuney [b], Christophe Jégou [a], F. Gauthier-Lafaye [d]

[a] CEA Centre de Marcoule BP 17171 30207, Bat 166, BP 17171, 30207 Bagnols sur Cèze cedex, France
[b] Nancy-Université, G2R, CNRS, CREGU, BP 239, 54506, Vandœuvre-lès-Nancy, France
[c] CRPG-UPR 2300 CNRS-Centre de Recherches Pétrographiques et Géochimiques, 54506 Vandoeuvre lès Nancy, France
[d] Centre de Géochimie de la Surface, EOST, CNRS/ULP, 1 rue Blessig, 67083 Strasbourg, France

ARTICLE INFO

Article history:
Received 14 November 2007
Accepted 6 May 2008

ABSTRACT

The issue of nuclear waste management – and especially spent fuel disposal – demands further research on the long-term behavior of helium and its impact on physical changes in UO_2 and $(U,Pu)O_2$ matrices subjected to self-irradiation. Helium produced by radioactive decay of the actinides concentrates in the grains or is trapped at the grain boundaries. Various scenarios can be considered, and can have a significant effect on the radionuclide source terms that will be accessible to water after the canisters have been breached. Helium production and matrix damage is generally simulated by external irradiation or with actinide-doped materials. A natural uranium oxide sample was studied to acquire data on the behavior of radiogenic helium and its diffusion under self-irradiation in spent fuel. The sample from the Pen Ar Ran deposit in the Vendée region of France dated at 320 ± 9 million of years was selected for its simple geological history, making it a suitable natural analog of spent fuel under repository conditions during the initial period in a closed system not subject to mass transfer with the surrounding environment. Helium outgassing measured by mass spectrometry to determine the He diffusion coefficients through the ore shows that: (i) a maximum of 5% (2.1% on average) of the helium produced during the last 320 Ma in this natural analog was conserved, (ii) about 33% of the residual helium is occluded in the matrix and vacancy defects (about 10^{-5} mol g^{-1}) and 67% in bubbles that were analyzed by HRTEM. A similar distribution has been observed in spent fuel and in $(U_{0.9},Pu_{0.1})O_2$. The results obtained for the natural Pen Ar Ran sample can be applied by analogy to spent fuel, especially in terms of the apparent solubility limit and the formation, characteristics and behavior of the helium bubbles.

1. Introduction

From the perspective of a deep geological repository for spent fuel it is essential to assess the impact of alpha self-irradiation on the long-term stability of the irradiated ceramic. The accumulation of irradiation damage and helium by radioactive decay of the actinides could modify the ceramic microstructure after several thousand years, allowing radionuclide release when water comes into contact with the fuel. These changes are likely to be of greater magnitude for high-burnup UO_2 fuel and for $(U,Pu)O_2$ MOX fuel with high actinide concentrations, especially in plutonium-rich aggregates.

These issues were already a subject of investigation in France under the terms of the Bataille Act of 1991 concerning radioactive waste management. The fifteen-year research period specified in that law expired in 2006; a subsequent waste management act in June 2006 temporarily extended the long-term behavior studies of spent fuel in a nuclear waste repository, and highlighted the need for further data on the long-term behavior of helium.

With regard to helium behavior, two scenarios directly related to its mobility under alpha self-irradiation at low temperatures can be considered: either the helium remains occluded in the matrix or trapped at the grain boundaries where it could eventually form inter- or intragranular microcracks liable to induce grain decohesion, or the helium is easily released from the ceramic and can accumulate in the fuel rods. The first scenario is the most challenging in a spent fuel repository because a significant increase in the fuel surface area would have a major effect on the two main source terms: instant release of radionuclides located outside the $(U,Pu)O_2$ grains and radionuclides located in the $(U,Pu)O_2$ matrix [1–3].

Many studies of helium behavior and disposition are based on simulated aging methods involving external irradiation by heavy ions or materials doped with short-lived actinides (^{244}Cm or ^{238}Pu) [4–6]. The basic data on thermal diffusion of helium in UO_2 [7–9] confirm that atomic thermal diffusion is nil over the time and temperature range of a disposal repository or in interim storage. Moreover, some observed phenomena, such as the discrepancy between microscopic and macroscopic volume expansion versus the damage level [4], require further investigation of helium behavior and its subsequent evolution.

* Corresponding author. Tel.: +33 466 796 172; fax: +33 466 797 708.
E-mail address: danielle.roudil@cea.fr (D. Roudil).

0022-3115/$ - see front matter © 2008 Elsevier B.V. All rights reserved.
doi:10.1016/j.jnucmat.2008.05.001

Irradiation damage has a major impact on helium mobility, and especially on thermal desorption. Fast helium mobility in all spent fuel or Pu-doped samples has been demonstrated above 700 or 800 °C [5]. At room temperature with strong instantaneous activity, helium can be also highly mobile; this can be attributed to a purely athermal diffusion mechanism arising from the instantaneous alpha activity [10,11].

To supplement the existing data concerning the intrinsic evolution of spent fuel, a novel alternative approach is to study natural uranium oxides with very ancient crystallization ages that can be considered as natural analogs. Although little or no work has been done specifically on helium diffusion in natural uranium dioxide crystals, helium diffusion has been evaluated for thermochronology studies in several natural mineral species [12–14]. Recent published articles have shown renewed interest in such samples, particularly from Oklo (Gabon), and their use as analogs of spent fuel in a geological nuclear waste repository [15,16].

Ancient uranium oxides often exhibit a complex geological history as a result of their high reactivity with the fluids that have interacted with them. The changes arising from these events (dissolution, oxidation, or formation certain phases) affect the subsequent helium mobility. The uranium oxides from Pen Ar Ran (France), with a concordant age of 320 million years were chosen for the first part of this study because of their relatively simple geological history.

The methodology consisted first in complete characterization of the minerals for fine analysis of their structure, chemical composition and crystallization ages. These data describe the history of the samples and the alteration process. They also allow a theoretical evaluation of the damage level and the helium production that will be compared with the helium desorption analysis results in terms of the overall balance and diffusion coefficients. Characterization by transmission electron microscopy before and after heat treatment allows to determine or corroborate helium localization in the material.

2. The Pen Ar Ran deposit

The sample studied is pitchblende a botroyoidal form of uranium oxide from the Pen Ar Ran deposit located near Piriac, a village in the Vendee region of France [17,18]. It was selected because of it is one of the best preserved from secondary alteration generally affecting natural uranium oxides. The uranium mineralization is located in an East–West fault crosscutting metamorphic formations at the northern edge of the Hercynian Guerande leucogranite. Mineralized veins cut acidic volcanics (ignimbrites) known as 'porphyroids' close to the contact with quartzitic and graphitic schists [19]. The mineralization consists of very homogeneous and massive uranium oxides (Fig. 1). A concordant U–Pb age of 320 ± 9 Ma [20] was obtained from ion microprobe isotopic analyses.

Mineral deposition in the sample starts with a comb of idiomorphic quartz crystals (a 2 mm thick gray band) which grew on a fracture wall cutting through the porphyroids (circle in Fig. 1). The heads of quartz crystals are first covered by a thin band (2 mm) of pitchblende spherules (uranium oxide). A thicker band (>1 cm) is then deposited symmetrically on the other side of the fracture; this band has a prismatic structure (tending to develop its cubic own forms), but with spheroid terminations. A fine sulfide band (1 mm) is present between the two uranium oxide bands.

The concordant U–Pb ages and the homogeneity of the rare earth element patterns (Fig. 2) in the uranium oxides corroborate the simple geological history of the Pen Ar Ran deposit compared with other uranium deposits throughout the world. Moreover, the Ar–Ar age of sericite in the surrounding metamorphic rock suggests that the Pen Ar Ran deposit was not subjected to any thermal event exceeding 300 °C after its deposition [21]. Thoria concentration remains low and not detectable by electronic microprobe. This is generally the case for low temperature natural oxides. On the other hand, calcium and lead concentrations are high in the oxide (between 1.32 and 9.56 wt% of CaO). These elements, lead in particular, should have an impact on diffusion properties.

According to [28] the structural formula of uraninites is

$$(U^{4+}_{1-x-y-z}U^{6+}_{x}REE^{3+}_{y}M^{2+}_{z})O_{2+x-(0.5y)-z} \quad (1)$$

Oxygen stoichiometry evolves with the nature and content of incorporated cations (tri and divalent). These oxidation level leads to a large amount of interstitial defect types. Their impact on diffusion properties have to be considered and isolated for UO_2 nuclear fuel comparisons.

Based on U–Pb age determination (320 ± 9 Ma) the total helium production can be estimated with allowance for decay of uranium (mainly ^{238}U) and of the principal -emitting decay products: ^{234}U, ^{230}Th, ^{226}Ra, ^{222}Rn, and ^{218}Po. A mean value of $8.125 \times 10^{20} \pm 2 \times 10^{19}$ $He/g_{UO_{2+x}}$ was determined. Assuming 1500 defects per disintegration reaction, the damage level reached is 182 ± 4.5 dpa*.

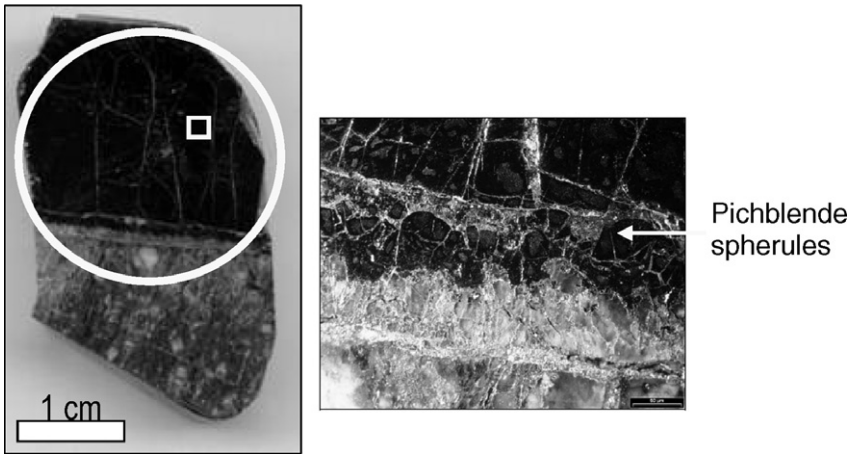

Fig. 1. Localization of the polished section cut in the sample (white circle). White square: TEM sampling area.

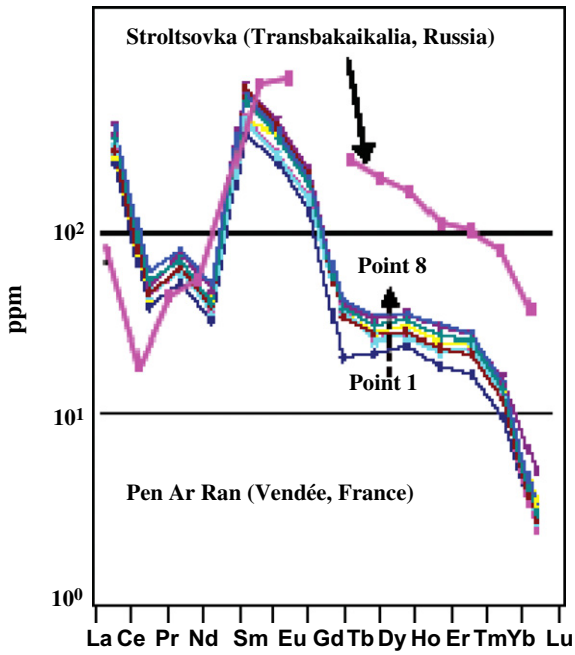

Fig. 2. Chondrite-normalized REE spectra of pitchblende in deposits at Pen Ar Ran (Vendée, France) and Streltsovska (Transbaikalia, Russia, volcanic).

3. Experimental setup

3.1. Helium desorption analysis system

The samples were wrapped in tungsten foil with a surface area of about 0.5 cm^2, which was then placed in an ultra-vacuum chamber at the top of a supporting thermocouple, about one centimeter from the window sealing the top of the chamber. This system allowed the sample to be heated by a halogen lamp placed outside the enclosure above the window. The lamp power was controlled by a regulator driven by a thermocouple to maintain a precise temperature at each stage of the experiment.

The system was very effective for measuring diffusion steps: the close proximity of the thermocouple and sample ensured very precise temperature control; only the sample received a significant quantity of heat, minimizing the increasing and decreasing temperature ramp effects. The selectivity of the heated zone also made it possible to use very low line blanks of about 8×10^{-15} moles. The evolved gas was first purified over a hot Ti-getter and a charcoal trap held at liquid nitrogen temperature. The released helium was then measured using a mass spectrometer calibrated with a standard ^{4}He sample. The concentrations were measured with 2% precision. At the end of each experiment, complete extraction was performed at high temperature to release all the gas remaining in the matrix. The temperature was maintained at 1000 °C until the instantaneous He concentration becomes nil.

For the helium desorption experiments analyzed by mass spectrometry, the Pen Ar Ran samples were taken from the massive oxide band. Measurements were carried out during increasing temperature steps lasting 20–30 min.

The ultra-vacuum first realized in the analysis chamber leads to an oxygen partial pressure between 10^{-6} and 10^{-8} Pa, according to air initial atmosphere. With this system, the sample is directly heated but not the surrounding media. According to literature data on UO_2, the oxygen potential could correspond to a highly oxidized UO_{2+x}. For a temperature range between 100 °C and 1000 °C, the O/U ratios remain greater than 2.2. Maintaining hyperstoichiometry of this oxide during thermal treatment is of major importance for our diffusion studies. Ab initio calculations [22] showed that the lowest energy solution site in UO_2 for rare gases depends on stoichiometry, namely U-vacancy for over stoichiometry, UO_{2+x}.

3.2. Helium release data processing

The diffusion coefficients were calculated from the diffusion measurements based on the model described in [23], which was specially derived for this type of multianalysis of a single specimen at successive temperature steps. The initial concentration profile in the sample is assumed to be uniform, and the diffusion coefficient calculated for each temperature step takes into account the new initial state at each step (an increasing concentration gradient from the core to the edge as the experiment progresses).

The diffusion profiles obtained for each experiment are plotted on classical Arrhenius diagrams in which the diffusion coefficient versus the temperature defines a straight line if the increase is an exponential function of the temperature. Under these conditions the diffusion parameters – the activation energy (E_a) and the infinite-temperature diffusion coefficient (D_0 is a pre-exponential frequency term) – can be determined experimentally from the following relation:

$$D = D_0 \times \exp\left(-\frac{E_a}{RT}\right) \quad (2)$$

Here, as routinely done in other studies, we have represented the reduced diffusion coefficient (D/a^2) rather than (D) to eliminate the effect of the grain size.

3.3. TEM experiments

A thin band was obtained on natural uranium oxide by digging into the sample with a gallium ion source under vacuum using an ion gun set up in a Philips FIB 200 transmission electron microscope (TEM) used in focused ion beam (FIB) mode. The thin uranium oxide band measured 15×5 μm and was about 100 nm thick. This thin band was made perpendicular to a microscopic crack and parallel to the mineral growth axis in order to cut across growth zones. A JEOL JEM 2010F High-Resolution transmission electron microscope equipped with energy-dispersive X-ray spectroscopy (EDS: Kevex) and electron energy loss spectroscopy (ELS: Gatan Imaging Filter) was used for observations.

3.4. Experimental samples

Helium diffusion was measured at up to 1000 °C on four uraninite specimens 300–500 μm in diameter, designated Pen Ar Ran I to Pen Ar Ran IV. The ratio of helium produced to helium conserved in the uranium oxides was accurately determined by (U–Th)/He datation [14] with three extractions at higher temperatures. Specimens of very different sizes, weighing from 50 to 625 μg, were placed in small (<1 mm diameter) platinum tubes and transferred to an ultra-vacuum chamber with filaments capable of heating the tubes to temperatures above 1300 °C for 45 min. These specimens were designated URAN-1, URAN-2 and URAN-3.

The total conserved helium balance was also determined by submitting samples to two heating protocols for more intensive systematic stripping: one series at 1400 °C on samples designated URAN-4, URAN-5 and URAN-6, and a second series at up to 1600 °C using a CO_2 laser on samples designated Laser-1 to Laser-4. Table 1 indicates the general characteristics of the samples analyzed in this study.

Small parts of Pen Ar Ran and URAN specimens were cut and used for the different TEM analysis.

Table 1
Results of ^{4}He extraction from Pen Ar Ran uraninite

Sample	Diam (μm)	Weight (mg)	E_a (kcal/mol) low-T	D_0 (cm^2/s) low-T	^{4}He (mol/g)	Age U/He (Ma)	% He conserved
Pen Ar Ran-I	300	0.167	35.6	8.1E+04	8.64E−06	1.8	0.6
Pen Ar Ran-II	324	0.239	40.4	9.7E+06	1.36E−05	2.9	1.0
Pen Ar Ran-III	296	0.172	31.3	1.3E+03	1.06E−06	0.2	0.1
Pen Ar Ran-IV	479	0.558	38.7	8.6E+04	1.22E−05	2.6	0.9
URAN-1	520	0.625	–	–	6.53E−05	13.9	4.7
URAN-2	337	0.254	–	–	3.04E−05	6.5	2.2
URAN-3	206	0.049	–	–	2.00E−05	4.2	1.4
URAN-4		0.234	–	–	3.64E−05	7.7	2.6
URAN-5		0.159	–	–	3.63E−06	0.8	0.3
URAN-6		0.124	–	–	9.77E−06	2.1	0.7
Laser-1		0.499	–	–	2.55E−05	5.4	1.8
Laser-2		2.097	–	–	2.11E−05	4.5	1.5
Laser-3		1.420	–	–	1.59E−05	3.4	1.1
Laser-4		2.170	–	–	5.96E−05	12.7	4.3

4. Results and discussion

4.1. Helium release measurements

Four diffusion experiments were carried out for a total of about 70 measurements between 100 and 1000 °C. The quantities released at low temperatures were 5–10 times higher than the measured line blank values, and above 200 °C they were several orders of magnitude higher.

The heat treatments applied to the Pen Ar Ran samples showed that practically all the helium produced in the matrix had been released naturally. The process is compatible with the very high diffusivity values observed at low temperatures (100–300 °C) in these experiments. During a longer temperature residence time (45 min) at 1300 °C a larger quantity of ^{4}He was released from the samples URAN-1, 2 and 3 (some 3–6 times more than the sum of all the preceding steps at temperatures lower than 1000 °C). Table 1, Figs. 3 and 4 show that all the helium was released at 1300 °C. The systematic stripping did not increase the results. Although the range was relatively heterogeneous, this approach confirmed that no more than 5% of the helium produced (2.1% on average) over about 320 Ma in this natural analog was conserved within the matrix. The activation energies and diffusion coefficients reflect the competition between bulk diffusion and rapid release of strong concentrations through defects.

Because of the small size of the samples, the possible recoil losses after the 10 μm range of the alpha particles has to be taken into account. Considering both a cylinder or parallelepiped sample cut into the mineral, and maximum losses in the first 10 μm near the surface less than 50% of the quantity of helium particle generated, we roughly estimated that this zone represented less than 10^{-4} to 3×10^{-4} at.% of the total helium generated and about 0.01% of the total quantity of helium retained. These calculations confirmed that in our experiments, the losses due to the range of the α particles is negligible in the helium released balance.

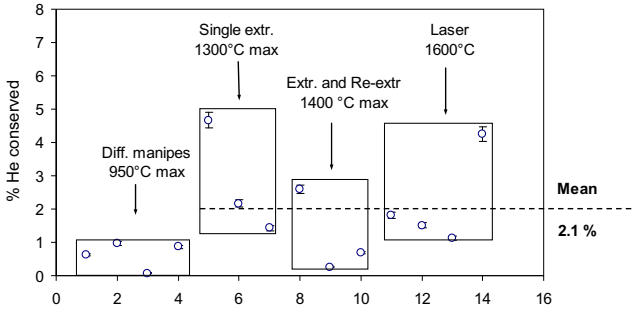

Fig. 3. Quantity of helium released for the Pen-Ar-Ran sample using different extraction techniques (in percent of total helium produced in the mineral since its formation).

Despite their age, the high mobility confirmed even at low temperatures by desorption experiments was enhanced by

- a *diffusion mechanism* that was purely athermal or activated by the presence of vacancy defects arising from self-irradiation [24,25]; the large quantity of defects being clearly visible by high-resolution imaging in Figs. 5 and 6.
- The deviation of the samples from stoichiometry due to an auto-oxidation process induced by UO_2 disintegration to PbO [26]. In general most of the uraninites are $UO_{2,m}$ oxide types, with m value distributed from 2.14 to 2.5. The excess oxygen is interstitial and the cubic phase is maintained at room temperature.
- The presence of an appreciable quantity of radiogenic and non-radiogenic lead and calcium (a few weight percent).

The reduced diffusion coefficients in these natural uranium oxides were 2–3 orders of magnitude higher than those obtained with synthetic UO_2 implanted with ^{3}He [9]. The reduced diffusion coefficients observed at temperatures above 800 °C were comparable to those (about 10^{-3} to 10^{-4} s^{-1}) obtained during similar experiments at ITU on spent fuel and doped UO_2 [5]. At these temperatures vacancy defects created by decay in UO_2 [4] were completely recovered, allowing release of the trapped helium. Similar behavior was observed on natural uranium oxides. In particular, experimental results presented in [27–29] showed two main stages in the thermal recovery of this polycrystalline materials:

- over 225 °C, oxygen interstitials migration,
- over 675 °C uranium vacancies, and associated helium atoms, migration.

For a thermal treatment at 1000 °C the lattice parameter is entirely recovered.

Our desorption experiments resulted in significant helium releases. For the Pen Ar Ran uranium oxides the distribution can be estimated at about 33% occluded gas in the matrix and vacancy defects, and 67% localized in bubbles (gas fraction released between 1100 and 1300 °C). A similar distribution has been observed in spent fuel and in $(U_{0.9},Pu_{0.1})O_2$ [5].

Helium analyses performed by Angelini on $^{238}PuO_2$ pellets [30] showed a significant increase in diffusion at room temperature, most likely due to self-irradiation, rapidly revealed by the high activity. In the case of uranium oxides, the room temperature mobility appears to be related to the sample conservation time.

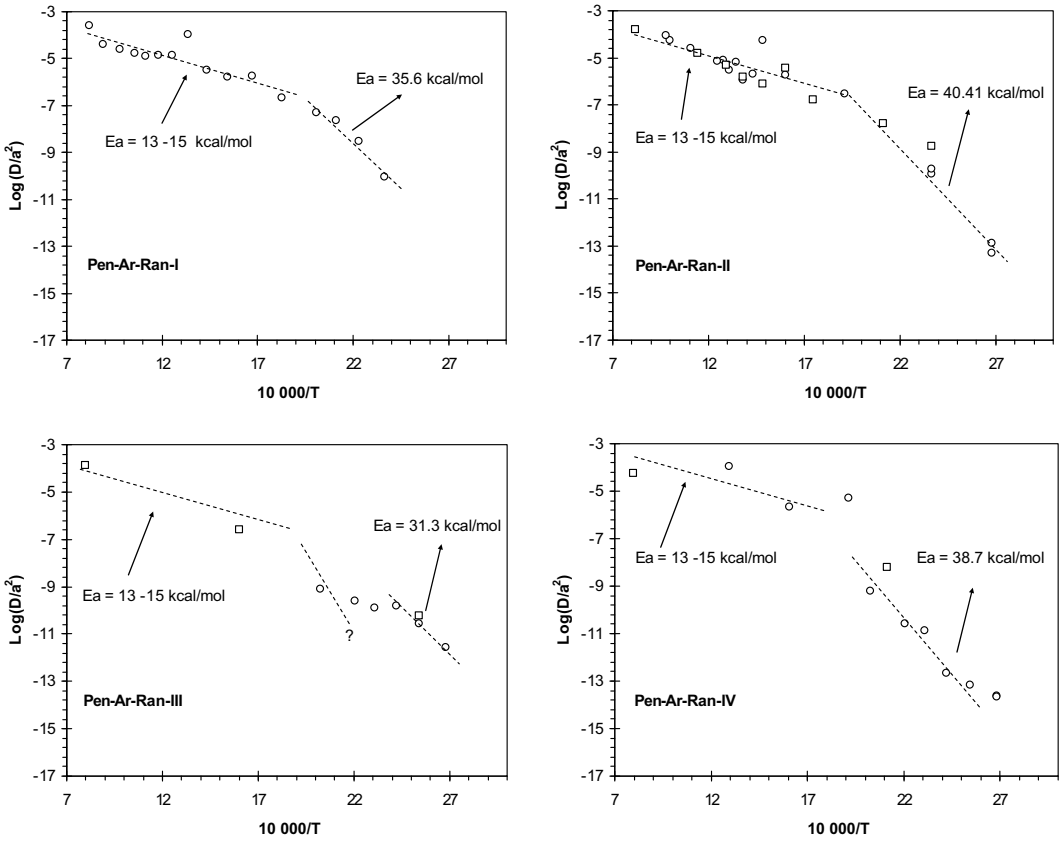

Fig. 4. Diffusion profiles obtained at successive temperature steps; white circles: increasing temperature, white squares: decreasing temperature.

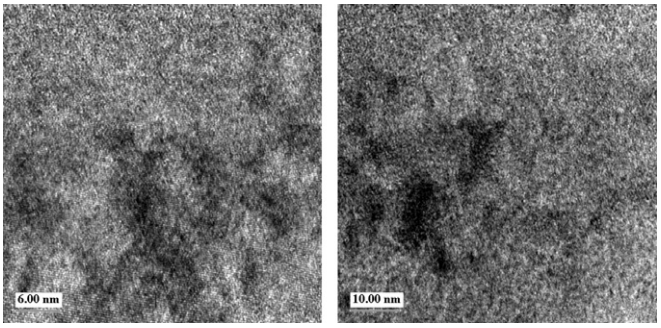

Fig. 5. High-resolution TEM images of damage zones in a raw sample.

The diffusion curves in Fig. 4 show a systematic change in slope at about 300 °C. At this temperature annealing of oxygen interstitials and vacancies is only obtained. In the higher temperature region the activation energy of helium diffusion is low (about 0.7 eV/at). Conversely, at low temperatures the release from uraninite is a continuous phenomenon. The activation energy measured below 300 °C is 1.7 eV/at; this appears to be the release of helium available near the surface or in the grain boundaries. The corresponding cumulative fraction remains very low, about 3–4% of the total helium analyzed.

At room temperature the reduced diffusion coefficient can be estimated by linear regression at $10^{-15}\,s^{-1}$; in fuel with a mean grain size of 10 μm, this corresponds to a diffusion coefficient of $2.5 \times 10^{-26}\,m^2\,s^{-1}$ at room temperature. This diffusion curve profile appears to reveal the impact of irradiation defects on helium mobility. Helium is gradually released above the 300 °C temperature threshold and up to 1100 °C.

This helium behavior versus temperature was also observed [31] when helium was analyzed in zircon for (U–Th)/He thermochronology measurements. The temperature threshold between the two ranges was 650 K and the activation energies were comparable to those determined here. The reduced diffusion coefficients were lower in zircon: $2.5 \times 10^{-8}\,s^{-1}$ at 500 °C for example.

The proportion occluded in the uraninite grains and fully released at temperatures below 1000 °C (lattice and defects) corresponds to a concentration of $10^{-5}\,mol\,g^{-1}$; this quantity of helium (6.4×10^{18} per gram of uraninite, or 0.1 atomic percent) could represent the solubility limit in UO_{2+x}. This low value is consistent with published values for the solubility of He in UO_2, between those determined in [32] and in [9].

4.2. Helium localization (TEM analysis)

4.2.1. Unannealed sample

The three sample zones indicated in Fig. 2 were examined. The zones sampled in pitchblende have identical structures and contain a large number of small, scattered helium bubbles forming clusters and strings (Fig. 6).

The examination of this sample revealed several features. The uranium oxide seems to be formed by a pile of successive layers 50–100 nm thick, in which the lattice is differently oriented, but appears to be very continuous in the clearest areas. This pile is perpendicular to the direction of the mineral growth. Some domains present more complex lattice orientations and/or variable defects in the structure organization).

Lead-rich segregations, well crystallized (50–70 nm), are observed mainly in the layer boundaries. They may be Pb or PbO, whereas PbS is unlikely (Fig. 6a). Many small spherules are observed (Fig. 6b), very frequent at the interfaces between bands

but also distributed throughout the sample. Because of the similarity of the microanalysis inside and outside the spherules (Figs. 6 and 7), we can considered that the bubbles contained only light elements, (H, He, Li). In this kind of samples submitted to uranium decay during very long periods, He is the more probable.

Very frequent helium bubbles (Fig. 6b) also develop preferentially but not exclusively at the band interfaces. Their size (generally about one nanometer) can reach ten nanometers in some aggregates. They are organized in constellations or honeycomb stitches, but sometimes form strings of nearly contiguous bubbles that are more or less continuous. If the contiguous helium bubble strings can represent preferential pathways for radiogenic helium release from the uranium oxides structure, isolated bubbles constitute much more effective traps for high temperature helium retention.

4.2.2. Sample annealed at 1000 °C

A thin section was sampled from a chip previously heated to 1000 °C. The first observation concerns the structure, which appears to be relatively unchanged after heating, except that it contains fewer defects – and some zones no longer contain any defects. Several dark spherules are visible: the spectra for these

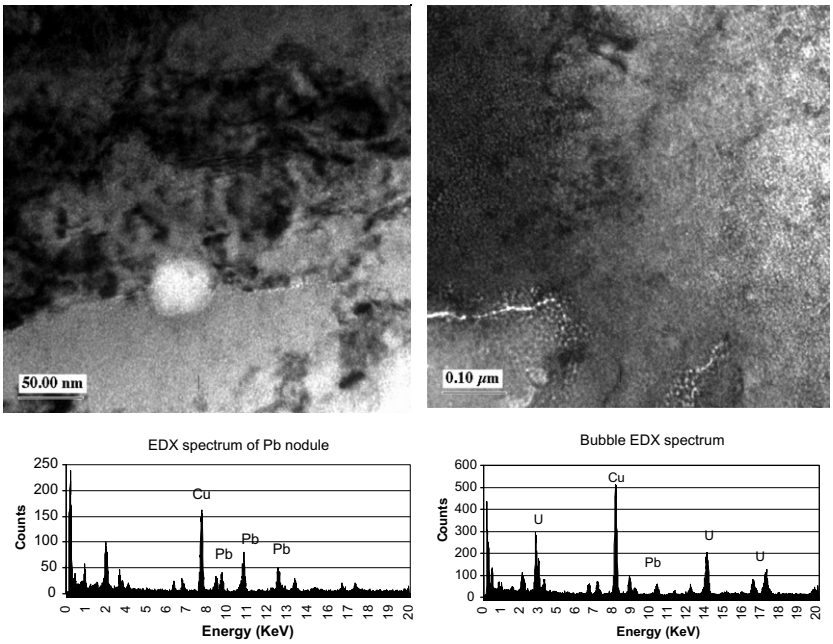

Fig. 6. (Left) Lead nodule in Pen-Ar-Ran sample and EDX spectrum. (Right) TEM image showing strings and clusters of small helium bubbles and EDX spectrum of bubbles.

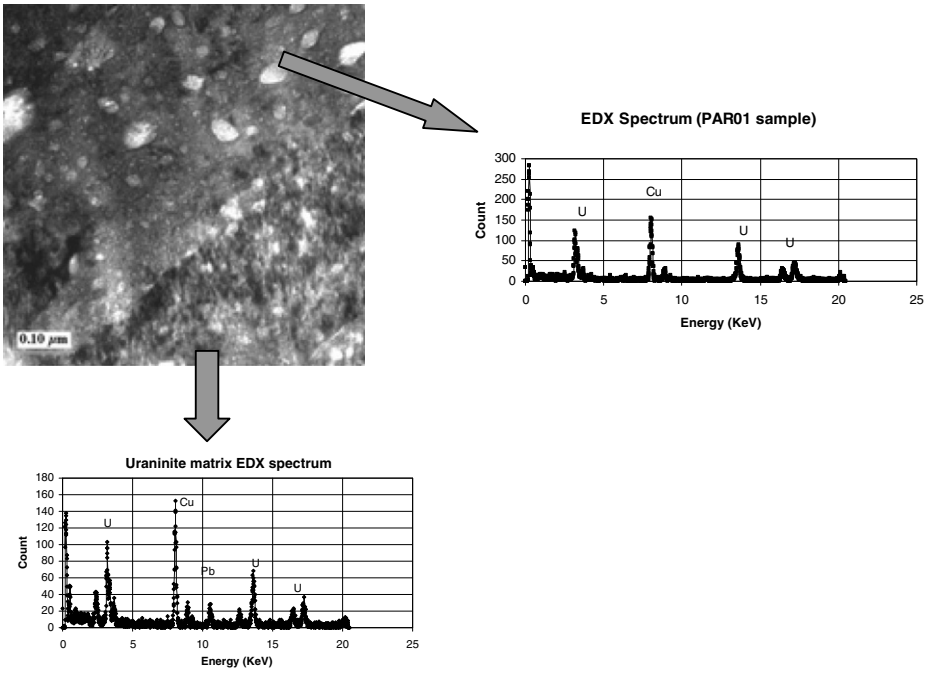

Fig. 7. Large helium bubbles of various shapes disseminated in the matrix after annealing at 1000 °C: EDX spectra of matrix and bubble.

zones clearly show that these are lead nodules. The dark coloration of the nodule may be due to the orientation of the section with respect to the beam.

Light-colored aggregates (Fig. 7) are observed throughout the specimen, very numerous, much larger than in the unannealed sample (about 20 nm) and in a variety of shapes. These observations suggest the coalescence of small bubbles under heating. Nevertheless, small spherical bubbles remain in some areas, but at a much lower concentration than in the unannealed sample. EDS analyses (Fig. 7) were identical for the matrix and for these bubbles, which therefore contain helium gas. Only Pb depletion was systematically detected.

4.2.3. Sample annealed at 1300 °C

The annealed sample in Fig. 8 exhibits high porosity, with large bubbles a few hundred nanometers in diameter. Microcracks are systematically observed near the bubbles. Contrary to the sample annealed at 1000 °C, all the small bubbles appear to have coalesced. The electron diffraction image is of a sample grain limited by microcracks: the uraninite atomic structure appears well ordered in this zone. No lead nodules can be observed here, nor was lead detected by EDS analysis. Fig. 9 shows an EDS spectrum of the matrix consisting of U and O together with a spectrum measured in the cavities.

The overall desorption analysis coupled with TEM characterization thus shows that heat treatment for 45 min at 1300 °C leads to complete release of the occluded helium. Following this extraction the traces of the cavities in which helium was trapped can be observed. They became filled with gallium when the thin sections were prepared for analysis by FIB with a gallium ion source (Figs. 8 and 9).

The trapped helium concentration in the bubbles represents 1–1.5 at.% of the helium generated, or about 1.9×10^{19} He g^{-1} based on high temperature desorption measurements. The bubbles coalesce at high temperature until they reach a critical size and concentration at which the helium is released. Microcracks appear around the edges of the bubbles after complete release. The maximum bubble size before release was about 600 nm for samples vacuum-annealed at 1300 °C. The wide dispersion of bubble sizes also reflects variations in the helium concentration.

According to the model described in [33] the minimum breakup pressure for the largest bubbles is 4.5 MPa. Solving the Van der Waals equation of state for this value gives a maximum concentration of less than 4.3×10^9 He atoms per bubble. For smaller bubbles, which also burst after annealing at 1300 °C, the most likely hypothesis is that their helium concentration is higher, for example, due to the coalescence of neighboring bubbles in clusters. Some bubbles are trapped by defects that appear to be mobile at 1000 °C and can thus coalesce more rapidly at lower temperatures.

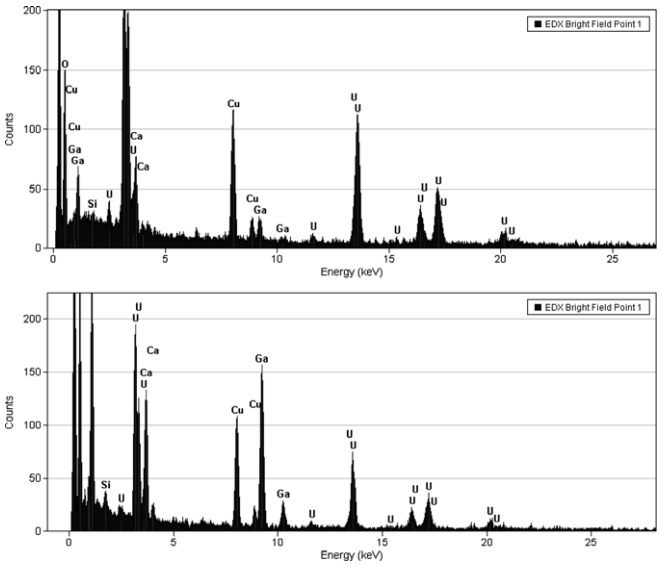

Fig. 9. EDX spectrum of uraninite and cavity after annealing at 1400 °C.

Table 2 summarizes the breakup pressure, atomic volume and helium concentration in the bubbles assuming release at 1300 °C from a homogeneous bubble population (size, He concentration). At room temperature and low pressure the bubbles are motionless. The number of bubbles and their pressurization at room

Table 2
Bubble variations in uranium oxides before and after heat treatment

	T = 1300 °C	T = 50 °C		
Bubble size (nm)	50	100	300	1
Pressure fail (Mpa)	26.7	13.4	4.45	1.67E+03
Vat (m^3)	2.29E−29	2.47E−29	2.60E−29	8.90E−29
He at./bubble	2.29E+07	1.69E+08	4.35E+09	4.71E+01
Bubbles/m^3	5.30E+18	7.00E+17	2.80E+16	2.00E+24

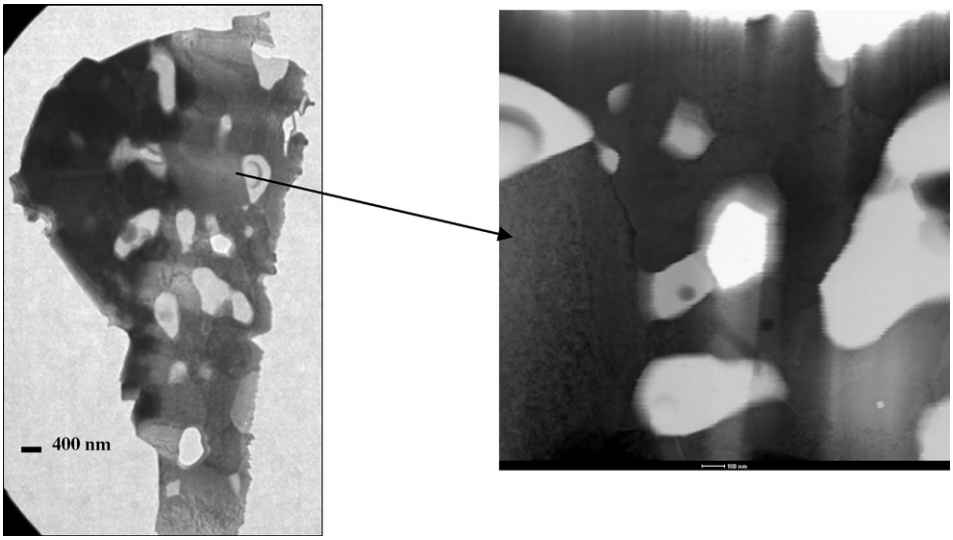

Fig. 8. Pen-Ar-Ran sample annealed at 1300 °C and zoom on the matrix showing few defect zone.

temperature could also estimated by image analysis based on TEM observations.

4.3. Extrapolation to spent fuel

Natural oxides of Pen Ar Ran showed two main phenomena, enhanced helium diffusion at low temperatures and formation of a high concentration of nanometric size bubbles.

For a total helium production of about 8.5×10^{20} at g^{-1}, the Pen Ar Ran uranium oxides exhibit not only strong natural release but also two possible helium locations: one in the matrix (solubilized helium or vacancy defects) with a mean concentration of 6.4×10^{18} at g^{-1}, the other in nanometric bubbles with a total concentration of about 1.9×10^{19} at g^{-1}.

Table 3 shows the helium production in different spent fuels during disposal in a repository. A total helium production of this magnitude can be reached only in MOX fuel over disposal time periods exceeding 50000 years, although this helium concentration is found in the Pu aggregates of MOX fuel after less than 5000 years. Conversely, if the maximum helium concentration analyzed in the matrix (6.4×10^{18} at/g) is considered as solubility limit, it will be reached very quickly: in 1000 years for UOX fuel (47.5 GWd t_{iHM}) but only about twenty years for MOX fuel with the same burnup.

These phenomena are exacerbated for Pu aggregates: bubbles can form very early and in large quantities. Under the thermal conditions prevailing in an interim storage facility or a geological repository, these defects – and thus the bubbles – exhibit extremely low mobility.

If this enhanced diffusion is considered as an effect of alpha damage, an increase of helium concentration, or partial release, at grain boundaries would be likely expected in nuclear spent fuels, in particular Pu aggregates. But under disposal conditions, taking into account both the duration of intrinsic evolutions and the diffusion coefficient values, we can also estimate that the major part of helium will remain trapped within the grain, in small bubbles. Mobility through bubbles in spent fuel appeared to be the main release mechanism. But the pores constitute potential traps for helium that can be released or dissolved only in the presence of a strong gas concentration and/or very high temperatures. These mechanisms are described with details in [24].

Table 3
Helium production in fuel after disposal

Mean He quantity (at g^{-1})			
Cooling time (years)	UOX (47.5 GWd t^{-1})	MOX (47.5 GWd t^{-1})	Pu aggregates of MOX
5			4.2×10^{18}
10	1.5×10^{18}	5.0×10^{18}	8×10^{18}
50			2.4×10^{19}
100	2.9×10^{18}	1.2×10^{19}	
1000	7.0×10^{18}	3.7×10^{19}	
5000	1.2×10^{19}	6×10^{19}	1.1×10^{20}
10000	1.4×10^{19}	7.7×10^{19}	
50000	2.5×10^{19}	1.2×10^{20}	

In UO_2 doped with 10 wt% $^{238}PuO_2$ fabricated at ITU, helium release measurements and TEM analyses [34] show that, for an integrated dose of less than 3.0×10^{18} α/g, helium remains mainly trapped in the grains in which nanometric bubbles already begin to appear. The apparent solubility limit appears to be similar in these less heavily damaged samples than in the natural uranium oxides.

At room temperature, however, strong instantaneous activity can induced important macroscopic damages. This was observed, for example, in sintered $^{238}PuO_2$ fabricated at CEA thirty years ago [2,35] as systematic grain decohesion, as shown in Fig. 10. Helium was produced in large quantities during this period, about 4.5×10^{20} α/g. A purely athermal diffusion mechanism arising from the instantaneous alpha activity, as reflected by a diffusion coefficient proportional to the instantaneous volume activity [11] leads to a high coefficient value, closed to 10^{-19} m^2 s^{-1}. But the initial high porosity (about 15%) should act as traps. Both helium mobility and alpha decrease defects can be involved in the observed damaging at the grain boundaries, probably through the accumulation of defects and/or coalescence of localized bubbles.

Table 4 summarized a comparison of apparent reduced diffusion coefficients at low temperature (100 °C) and diffusion path for uranium and plutonium oxide samples and Pen Ar Ran

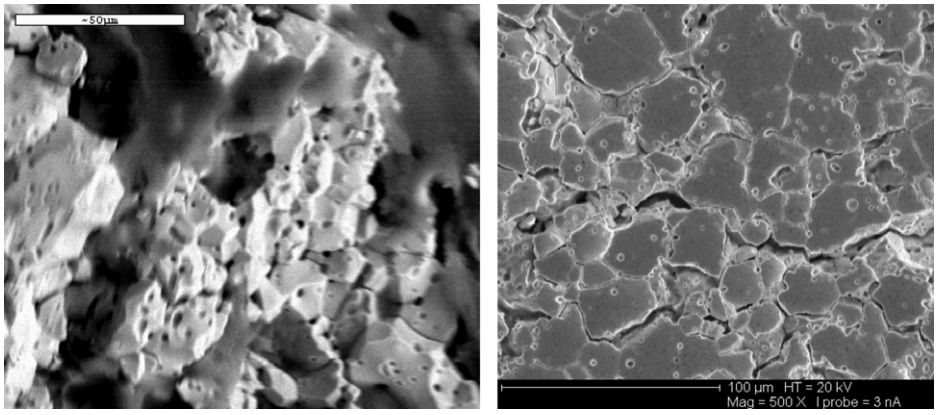

Fig. 10. SEM image of $^{238}PuO_2$ samples conserved for 30 years (from [34]).

Table 4
Diffusion path comparison between UO_2, $(U,Pu)O_2$ fuels and Pen-Ar-Ran oxides

Specimen	Reduced diffusion coef. at 100 °C (s^{-1})	Diffusion path (µm)				
		1000 y	10000 y	500000 y	100000 y	300 millions y
Pen-Ar-Ran	10^{-14}	0.18	0.28	0.63	0.9	48.6
$(U,Pu)O_2$ from [5]	3×10^{-23}	5×10^{-6}	1.5×10^{-5}	3.5×10^{-5}	5×10^{-5}	0.03
UO_2 from [9]	1.2×10^{-27}	3×10^{-8}	10^{-7}	2.2×10^{-7}	3.1×10^{-7}	1.5×10^{-5}

specimens. At this low temperatures the diffusion coefficient values are nine orders of magnitude higher in uraninites. But for temperature greater than 600 °C, reduced diffusion coefficients have closed values. This comparison confirms that during the intrinsic evolution period of disposal, atomic helium mobility should be very low and the formation and pressurizing of bubbles would then be very likely. The high porosity in Rim and Pu aggregate zones must also be taken into account.

5. Conclusions and outlook

This work confirms and supplements previous observations of helium bubbles in natural uranium oxides, as reported notably in [36,37].

One important conclusion that can be drawn from this study is the existence of two possible locations for the small occluded helium fraction in the matrix.

Vacuum heat treatment at up to 1000 °C of the Pen Ar Ran overstoichiometric oxides resulted in the rapid release of a fraction of the helium trapped in vacancy defects, and the coalescence of small helium bubbles initially found in clusters or strings. The bubbles grew to about 20 nm on average. The helium was released from the bubbles only at higher temperatures, near 1300 °C. Additional diffusion experiments with extended residence times at 1000 °C confirmed this release mechanism as well as the two locations determined for helium. Lead nodules were always present before and after annealing the Pen Ar Ran uranium oxide; they do not appear to be mobile at test temperatures.

The mechanisms governing the high mobility of helium at low temperatures are currently the subject of further investigation and analysis allowing for oxidation of natural uranium oxides and their high lead content. Nevertheless, the results obtained here can be applied by analogy to spent fuel in terms of the apparent solubility limit and the formation and behavior of the bubbles.

The helium concentrations corresponding to the last two parameters will very quickly be reached in spent MOX fuel and particularly in the Pu aggregates. Assuming lower helium mobility in the fuel under disposal conditions but in the time–temperature domain of intrinsic evolutions, the formation of large quantities of bubbles can be expected, eventually resulting in pressurization and/or coalescence as a result of their proximity.

This research protocol will now be applied to older samples, not only to confirm and supplement the data concerning the apparent solubility and the bubble formation and breakup mechanisms, but also using samples from Oklo (Gabon) to determine whether the damage initially generated during the criticality period has a significant impact on subsequent helium behavior. Very ancient samples crystallized about 2 billion years ago will provide further data on the bubbles size distribution when subjected to a very high integrated α dose.

Acknowledgments

This work was performed within the framework of a research program funded by the CEA (T. Lieven, C. Ferry) and EDF (J.M. Gras). The authors are especially grateful to Wahib Saikali of CP2M at P. Cézanne University in Marseille for the quality of his HRTEM analysis.

References

[1] C. Jégou, S. Peuget, V. Broudic, D. Roudil, X. Deschanels, J.M. Bart, J. Nucl. Mater. 326 (2004) 144.
[2] C. Ferry, C. Poinssot, C. Cappelaere, L. Desgranges, C. Jégou, F. Miserque, J.P. Piron, D. Roudil, J.M. Gras, J. Nucl. Mater. 352 (1–3) (2006) 246.
[3] D. Roudil, C. Jégou, V. Broudic, B. Muzeau, S. Peuget, X. Deschanels, J. Nucl. Mater. 362 (2007) 411.
[4] D. Roudil, C. Jégou, X. Deschanels, S. Peuget, C. Raepsaet, J.P. Gallien, V. Broudic, Mater. Res. Soc. Symp. Proc. 932 (2005) 529.
[5] C. Ronchi, J.P. Hiernault, J. Nucl. Mater. 325 (2004) 1.
[6] V.V. Rondinella, H.J. Matzke, J. Cobos, T. Wiss, Mater. Res. Symp. Proc. 556 (1999).
[7] S. Guilbert, T. Sauvage, H. Erranli, P. Desgradin, G. Blondiaux, C. Corbel, J.P. Piron, J. Nucl. Mater. 321 (2003) 121.
[8] S. Guilbert, T. Sauvage, Ph. Garcia, G. Carlot, M.-F. Barthe, P. Desgardin, G. Blondiaux, C. Corbel, J.P. Piron, J. Nucl. Mater. 327 (2004) 88.
[9] D. Roudil, X. Deschanels, P. Trocellier, C. Jégou, S. Peuget, J.M. et Bart, J. Nucl. Mater. 325 (2004) 148.
[10] C. Ferry, P. Lovera, C. Poinssot, P. Garcia, J. Nucl. Mater. 346 (2005) 48.
[11] P. Lovera, C. Ferry, C. Poinssot, L. Johnson, Synthesis report on the relevant diffusion coefficients of fission products and helium in spent nuclear fuels, CEA-Report, Personal communication, 2003.
[12] P.W. Reiners, K.A. Farley, Geochim. Cosmochim. Acta 63 (1999) 3845.
[13] K.A. Farley, J. Geophys. Res. 105 (2000) 2903.
[14] R. Pik, B. Marty, in: AGU, 1999 Fall Meeting, vols. 80, 46, 1999, p. 1169.
[15] S. Utsunomiya, R.C. Ewing, L.M. Wang, Letters 240 (2005) 521.
[16] L.Z. Evins, K.A. Jensen, R.C. Ewing, Geochim. Cosmochim. Acta 69 (6) (2005) 1589.
[17] J. Bonhoure, M. Cuney, Analyses in situ des Terres Rares et datation isotopique U–Pb des oxydes d'uranium du gisement de Pen Ar Ran (Vendée, France), Personal communication, 2005.
[18] M. Cuney, R. Pik, F. Gauthier-Lafaye, D. Roudil, Étude de la diffusion de l'hélium dans les oxydes d'uranium, Personal communication, 2006.
[19] M. Cathelineau, M. Cuney, J. Leroy, F. Lhote, C.T. Nguyen, M. Pagel, B. Poty, in: 'Vein Type and Similar Uranium Deposits in Rocks Younger than Proterozoic' Proceedings of Symposium Lisbon, 1979, IAEA, Vienna Edit., 1982, p. 159.
[20] P. Holliger, in: SIMS VIII, J. Wiley and sons, 1992, p. 719.
[21] F. Le Hebel, Déformation continentale et histoire des fluides au cours d'un cycle subduction exhumation extension, Exemple des Porphyro sud-armoricains, Unpublished Thesis, Rennes I, 2002, p. 25.
[22] J.P. Crocombette, J. Nucl. Mater. 305 (2002) 29.
[23] H. Fetching, S. Kalbitzer, in: Potassium–Argon Dating, O. Schaeffer, 1966.
[24] Hj. Matzke, Radiat. Eff. 53 (1980) 219.
[25] Hj. Matzke, J. Nucl. Mater. 114 (1983) 121.
[26] R.M. Berman, J. Mineral. Soc. Am. 42 (1957) 705.
[27] J.P. Stout, G.R. Lumpkin, R.C. Ewing, Y. Eyal, Mater. Res. Soc. Proc. 112 (1988) 495.
[28] R. Evron, G. Kimmel, Y. Eyal, J. Nucl. Mater. 215 (1994) 54.
[29] J. Janeczek, R.C. Ewing, J. Nucl. Mater. 185 (1992) 66.
[30] Angelini, Helium release from $^{238}PuO_2$ microspheres, ORNL-4507, 1970.
[31] M. Reich, R.C. Ewing, T.A. Ehlers, U. Becker, Geochim. Cosmochim. Acta 71 (2007) 3119.
[32] F. Rufeh, D.R. Olander, T.H. Pigford, Nucl. Sci. Eng. 233 (1965) 335.
[33] C. Ferry, J.P. Piron, Effet de l'accumulation d'hélium sur la microstructure du combustible usé en conditions d'entreposage et de stockage: État de l'art et premières évaluations, Personal communication, 2006.
[34] V.V. Rondinella, T. Wiss, Hj. Matzke, J.P. Hiernault, R. Fromknecht, in: Proc. Int. Conf. Mass and Charge Transport in Inorganic Materials, 2000.
[35] D. Roudil, X. Deschanels, M. Desir, P. Nivet, R. Caraballo, J.M. Boubals, M. Bojat, État physique des sources de $^{238}PuO_2$ après 30 ans de stockage, Personal communication, 2005.
[36] J.P. Stout, G.R. Lumpkin, R.C. Ewing, Y. Eyal, Mater. Res. Soc. Symp. Proc. 112 (1988) 495.
[37] R. Finch, T. Murakami, in: Reviews in Mineralogy, vol. 38, Uranium: Mineralogy Geochemistry and the Environment, 1999, p. 91.